Chinese Chemical Letters 31 (2020) 1839–1842

Contents lists available at ScienceDirect

Chinese Chemical Letters

journal homepage: www.elsevier.com/locate/cclet

Communication

Study of the effect of chemical composition on the surface wettability of three-dimensional graphene foams

Guihua Huang[a,1], Xinhong Song[c,1], Yiying Chen[b], Fangyuan Lin[b], Yipeng Huang[b], Feiming Li[b], Zhiyong Guo[a], Qiuhong Yao[a], Xi Chen[b,*]

[a] Institute of Analytical Technology and Smart Instruments, College of Environment and Public Health, XiamenHuaxia University, Xiamen 361024, China
[b] State Key Laboratory of Marine Environmental Science, Xiamen University, Xiamen 361005, China
[c] College of Ocean Science and Engineering, Shanghai Maritime University, Shanghai 201306, China

ARTICLE INFO

Article history:
Received 4 January 2020
Received in revised form 26 February 2020
Accepted 27 February 2020
Available online 28 February 2020

Keywords:
3D graphene foam
Surface wettability
Dopant configuration
Chemical composition
Aminobenzene sulfonic acid

ABSTRACT

The chemical composition obviously affects the surface wettability of a three-dimensional (3D) graphene material apart from its surface energy and microstructure. In the hydrothermal preparation, the heteroatom doping changes the chemical composition and wettability of the 3D graphene material. To realize the controllable surface wettability of graphene materials, aminobenzene sulfonic acid (ABSA) was selected as a typical doping agent for the preparation of nitrogen and sulfur co-doped 3D graphene foam (SNGF) using a hydrothermal method. Different from using *o*-ABSA or *p*-ABSA as the dopant, SNGF with tunable surface wettability is obtained only when *m*-ABSA is used. This result indicates that the substituent position of -SO_3H group in the benzene ring of ABSA is rather important for the tunable wettability. This work provides some theoretical foundations for dopant selection and some new insights in manipulating the properties of 3D graphene foams by adjusting the configuration of dopants.

Two-dimensional (2D) materials such as graphene, boron nitride, and black phosphorus nanosheets have attracted worldwide attention in recent years [1–5]. However, the poor stability, low porosity and low recovery efficiency of 2D nanosheets greatly obstacles their applications [6]. Differently, graphene-based aerogels and foams are interconnected three-dimensional (3D) graphene macroscopic monoliths, which maintain the property of graphene nanosheets as well as the macroscopic, 3D porous structure. Recently, 3D graphene materials have attracted much attention due to their excellent properties such as high surface area, excellent mechanical strength and mass transfer performance [7–10]. The electrical, optical, mechanical, catalytic properties and surface wettability of 3D graphene materials can be modified on the assembly processes. At present, most of the obtained 3D graphene materials are hydrophobic [6,11–14]. Liu *et al.* prepared magnetic polymers with 3D graphene, and the water contact angle (CA) of this product was 158° [15]. As Zhang *et al.* reported, a 3D graphene material with a water CA of 137° could be obtained after composited with fluoroalkylatedsilane [16]. Superhydrophobic 3D graphene aerogels were prepared by Zhang *et al.* by hydrothermal reduction of GO in the presence of dopamine followed by freeze-drying and pyrolysis [17]. The material presents good surface wettability to various oils, and the CA to water is above 150°. Generally, the hydrophilic oxygen-containing groups on graphene sheets are greatly reduced, and the number of conjugated benzene rings on the plane is increased after the reduction. The reduced 3D graphene often shows hydrophobic or superhydrophobic characteristic, which limits their applications in aqueous environments. Therefore, the surface wettability of 3D graphene materials should be effectively controlled in the assembly processes to expand the possibility of practical applications in aqueous environments.

The wettability of a 3D graphene material can be affected by many factors, such as the chemical composition, surface microstructure and surface energy. In terms of the chemical composition, the heteroatom doping is an effective approach to change the properties of 3D graphene foams for additional functions and applications [18,19]. The doped nitrogen (N), phosphorus (P), boron (B), sulfur (S) or other hybrid atom changes the band gap of graphene and affects the electrical properties of surrounding carbon (C) atoms, and thus destroys the electric neutrality of graphene surface [20,21]. Meanwhile, the doping of heterogeneous atoms causes the structural defects of graphene, then changes the

* Corresponding author.
E-mail address: xichen@xmu.edu.cn (X. Chen).
[1] These authors contributed equally to this work.

https://doi.org/10.1016/j.cclet.2020.02.053
1001-8417/

physical and chemical properties of the material. Compared with single heteroatom doping, multielement doping can obtain better physicochemical properties [22–24]. P/N co-doped 3D graphene aerogels was reported to show better conductivity and catalytic activity [25]. Another P/N co-doped 3D super-amphiphilic graphene foam was assembled using phytic acid (PAGF) and orphosphorylethanolamine (PNGF) as both gelling agent or/and dopant. The super-amphiphilic PAGF triggers the efficient epoxidation of alkenes without adding a co-solvent or stirring [26], and exhibits enhanced absorption capacity for Pb(II) and Cd(II) cations in water [27]. Improved electrochemical activity and catalytic performance have also been reported in N/B co-doped and P/N coldoped graphene [28]. Although heteroatom doping has frequently been used to modify graphene materials for improved performances, the influences of the configuration of dopants on the doping efficiency and the resultant properties of graphene materials have rarely been realized.

In this letter, we report the achievement in tunable surface wettability of N/S co-doped 3D graphene foam (SNGF) using *m*-aminobenzene sulfonic acid (*m*-ABSA) as the dopant. We systematically studied the effects of the configuration of ABSA on the surface wettability of N/S co-doped 3D SNGF, apart from the dosage of ABSA, the solution pH, and the annealing temperature, to reveal the importance of the configuration of dopants in the resulting material properties.

The graphene oxide (GO) was prepared by modified Hummer's method as described in literature [29,30]. For the preparation of N/S co-doped 3D SNGF, several amounts of ABSA were added into a GO aqueous dispersion (15 mL, 2 mg/mL). After the sonication (60 min), the mixture was sealed in a 20 mL Teflon autoclave for hydrothermal treatment at 180 °C for 12 h. After the reaction, the autoclave was naturally cooled to room temperature, then the product was taken out and rinsed with water for 3 times. The product was further purified by soaking in water for 24 h (the water was refreshed every 8 h), then freeze-dried for 24 h. Columnar N/S co-doped 3D SNGF was finally obtained after annealing for 1 h at 400 °C, 800 °C, or 1000 °C under argon atmosphere, and the products were denoted to SNGF/400, SNGF/800, and SNGF/1000, respectively.

The morphology of the SNGF was observed using scanning electron microscopy (SEM, Hitachi S4800) with an acceleration voltage of 15 kV and transmission electron microscopy (TEM, JEM-1400) with an acceleration voltage of 100 kV. X-ray photoelectron spectroscopy (XPS) were performed on a PHI Quantum 2000 XPS system (Physical Electronics, USA) paired with an Al Kα X-ray source (1486.6 eV), and the contaminated carbon C 1s (284.6 eV) was used as the standard for charge correction. All measurements of surface roughness were conducted using a VK-X200/VK-X200 (Keyence, Japan) and analyzed by VK-Analyzer software. Raman spectra were collected by a Nanophoton Raman 11 (Nanophoton, Japan) with an excitation wavelength of 532.00 nm, laser current of 100% and excitation power of 5.5 mW. The contact angles of a liquid on the 3D SNGF surface were measured with a Ramé-Hart 200-F1 goniometer (Ramé-Hart, USA) by advancing a drop of water or oil (3 μL) on the SNGF surface using a 2 mL micrometer syringe.

After the hydrothermal self-assembly, a cylindrical SNGF with a diameter of about 10 mm and a height of about 12 mm could be obtained. The macroscopic photographs of the 3D SNGF show no significant difference by using *o*-, *m*-, or *p*-ABSA as the doping agent (Fig. 1a). After freeze-drying, each SNGF has a mass of about 27 mg, indicating the lightweight property. SEM images (Figs. 1b-d) reveal similarly 3D macroporous structures in *o*-, *m*- and *p*-SNGF. The pore walls are composed of randomly crosslinked graphene nanosheets, and the inhomogeneous macropores are interconnected. TEM images of the three SNGF materials (Figs. 1e-g) also show similar wrinkles of the graphene sheets, which is consistent with previous reports [20,23,25].

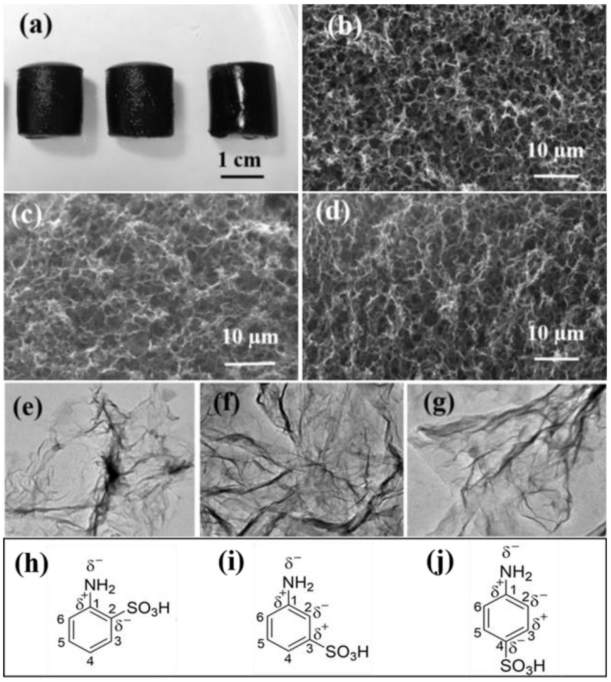

Fig. 1. (a) Macroscopic photographs of the *o*-SNGF (left), *m*-SNGF (middle) and *p*-SNGF (right). The SEM images of *o*-SNGF (b), *m*-SNGF (c) and *p*-SNGF (d). TEM images of images of *o*-SNGF (e), *m*-SNGF (f) and *p*-SNGF (g). The SNGF were all synthesized under the condition of ABSA/GO = 3/1 (mass ratio) and pH 3.4. The electron distribution in benzene ring for *o*-ABSA (h), *m*- ABSA (i) and *p*-ABSA (j).

As an effective tool, Raman spectroscopy was used to investigate the disorder degree of the 3D SNGF. The intensity ratio of the D band (1330 cm^{-1}) and G band (1585 cm^{-1}) (I_D/I_G) in the Raman spectroscopy is proportional to the disorder degree of a graphene material [31]. As shown in Fig. S1 (Supporting information), the ratio of I_D/I_G is 1.17, 1.24, 1.30 and 1.29 for GF, *o*-, *m*-, and *p*-SNGF, respectively. Compared with GF, the increased I_D/I_G value in SNGF well indicates the enhanced disorder after the introduction of N/S heteroatoms [32]. The close I_D/I_G values in *o*-, *m*- and *p*-SNGF indicate the similar disorder degree in the three SNGF. After high-temperature annealing, the I_D/I_G ratios of *o*-, *m*- and *p*-SNGF/1000 increase to 1.46, 1.51 and 1.47, respectively, indicating that the annealing treatment further changes the disorder degree of the graphene materials. In addition, the relative higher I_D/I_G ratio in *m*-SNGF suggests that more heteroatom atoms may be introduced by using *m*-ABSA.

Based on the above result, the effect of *o*-, *m*- and *p*-ABSA on the chemical composition of SNGF was further studied. High-resolution N 1s XPS spectra (Figs. S2a-c in Supporting information) reveal exists of some amino nitrogen (N-A) structure in *o*-SNGF/1000 and *p*-SNGF/1000. Differently, the nitrogen in *m*-SNGF/1000 has been completely transformed to pyridinic nitrogen (N-6) and graphitic nitrogen (quaternary-N, N-Q) structures. The S 2p XPS spectra (Figs. S2d-f in Supporting information) show that some oxidized sulfur (S-O) is retained in *o*-SNGF/1000 and *p*-SNGF/1000, but all S in *m*-SNGF/1000 exist in the form of thiophenic state sulphur (thiophene S, S-T). Different from the nucleophilic reaction between -NH_2 and the oxygen-containing groups on GO, the reactions between -SO_3H groups and GO is induced by electrophilic substitution of the H on the benzene ring at the edge of GO lamellar or esterification reaction with -OH on the GO. Therefore, reducing the electron density on the -SO_3H group in ABSA is conducive to improve the reactivity of the -SO_3H group with GO. As shown in Figs. 1h-j, different from the case in *o*- and *p*-ABSA, the electron density on the carbon directly connecting with -SO_3H group is

relatively positive in *m*-ABSA, leading to lower electron density on the -SO_3H group. The decreased electron density then activates the electrophilic reactivity of *m*-ABSA to GO. In hydrothermal reaction, compared with *o*-ABSA and *p*-ABSA, a higher proportion of -SO_3H groups in *m*-ABSA can directly bond to the GO lamina. Then in the subsequent annealing process, the bonded -SO_3H groups further reacted with rGO layer and doped into the graphene lattice to form S-T state. Inversely, the large amount of unbonded -SO_3H groups in *o*-ABSA or *p*-ABSA cannot further react with the graphene carbon. Some of them is thermally decomposed, and the other part was still retained in -SO_3H form. In addition, -SO_3H passivates the reactivity of the *o*-position or *p*-position -NH_2 on the benzene ring, which attributes the N-A form in *o*-SNGF/1000 and *p*-SNGF/1000, but N-6 or N-Q form in *m*-SNGF/1000.

Since the higher reactivity of *m*-ABSA has been demonstrated, the effect of *m*-ABSA/GO mass ratio on the SNGF structure was further investigated. Fig. S3 (Supporting information) shows the SEM images of GF, *m*-SNGF-1, *m*-SNGF-2 and *m*-SNGF-3 with *m*-ABSA/GO mass ratio of 0, 1, 2 and 3, respectively. The four materials all show typical porous structure of 3D graphene. With increasing ABSA/GO mass ratio, the pore diameter of *m*-SNGF tends to be increased because more gas was released by using more ABSA. The ratio of I_D/I_G increases from 1.21 to 1.30 when the mass ratio of ABSA/GO is changed from 1 to 3 (Fig. S4 in Supporting information), indicating that the higher ABSA/GO ratio results in higher disorder degree. After the annealing, larger pores and higher disorder degree are also found in the sample that prepared using higher ABSA/GO ratio (Fig. S5 in Supporting information). The results indicate that higher amounts of ABSA improve the porosity and looser structure of the SNGF. XPS spectra (Fig. S6 in Supporting information) of *m*-SNGF/1000 with different ABSA/GO ratio are rather similar, however, the higher ABSA/GO ratio contributes to overall higher amounts of doping heteroatoms. N 1s and S 2p XPS spectra reveal that the N exists in the form of N-6 and N-Q, and all S exists in the form of S-T, indicating that the ABSA/GO mass ratio does not affect the doping form of heteroatoms in the *m*-SNGF/1000.

To study the effect of pH on the morphology of the resultant *m*-SNGF, the pH value of the hydrothermal solution ranging from 3.4–10.0 were investigated. Fig. 2a illustrates that the size of the resulting SNGF is gradually enlarged with increasing pH value. The SNGF is rather loose and fragile when the pH value is 10.0. SEM images (Figs. 2b-d) further confirm that higher pH value attributes to larger pores and discrete pore walls. The weak interconnection in pore wall then results in the structural collapse. As shown in Figs. 2e-g, when the water droplet contacts to the *m*-SNGF surface, the droplet immediately spreads out on the *m*-SNGF surface because of the hydrophilicity of the *m*-SNGF. The *m*-SNGF synthesized at pH 3.4 shows unobserved surface change after the contact with water droplet. However, the surface of the *m*-SNGF synthesized at pH 7.0 appears slightly depressed after contacting with water droplet. The surface collapse becomes obvious for the *m*-SNGF synthesized at pH 10.0 solution. The results indicate that the preparation of *m*-SNGF under an acidic condition ensures the integrity and stability of the 3D skeleton.

The morphology, chemical composition, and wettability of SNGF at different annealing temperature (400 °C, 800 °C and 1000 °C) were also investigated. Interestingly, the SNGF is all about 20 mg though annealed at different temperature. SEM images show that higher annealing temperature causes larger pores, but the interior skeleton remains integrated and interconnected (Figs. 3a-d). Raman spectra show an increased trend in I_D/I_G value (from 1.30 for *m*-SNGF to 1.51 for *m*-SNGF/1000) with increasing annealing temperature (Fig. S7 in Supporting information). The result reveals that the heteroatoms are easier to dope in the graphene network at high temperature [27].

As shown in the Fig. S8 (Supporting information), the higher annealing temperature causes the more surface roughness due to the formation of the air columns which block water into the surface, resulting in the higher hydrophobicity of the material (Figs. 3e-h). To investigate the influence of annealing temperature on the chemical composition of SNGF, XPS spectra were collected. Fig. S9 (Supporting information) shows that the atomic percentages of O is significantly decreased after annealing mainly because the reduction of GO [33]. The atomic percentages for N and S also decrease after annealing due to the partially thermal decomposition of -NH_2 and -SO_3H. C 1s XPS spectra (Fig. S10 in Supporting information) indicate the forms of C=C (~284.8 eV), C—C (~285.1 eV), C—O (hydroxyl and epoxy groups, ~286.4 eV) and C=O (carbonyl group, ~289.1 eV) in *m*-SNGF [34]. As the *m*-SNGF was annealed from 400 °C to 1000 °C, the C—O and C=O components gradually decreases, explaining the decreased oxygen content. N 1s XPS spectra (Fig. S11 in Supporting information) show two different valence states, N-A (~401.5 eV) and pyrrole nitrogen

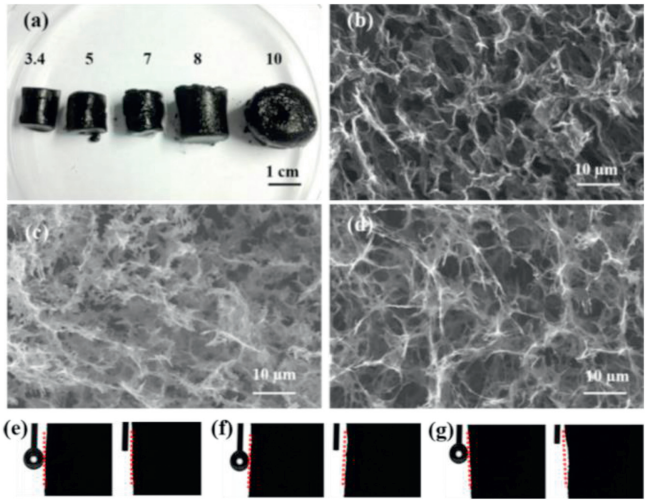

Fig. 2. (a) Morphologies of the *m*-SNGF prepared at pH of 3.4–10.0. The SEM image of the *m*-SNGF prepared at pH of 3.4 (b), 7.0 (c) and 10.0 (d). The surface of *m*-SNGF prepared at pH of 3.4 (e), 7.0 (f) and 10.0 (g) before and after the contact of a water droplet.

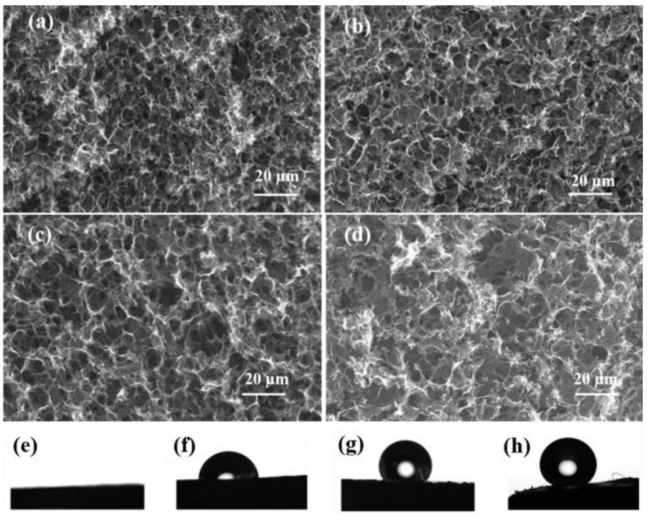

Fig. 3. The SEM image of *m*-SNGF (a), *m*-SNGF/400 (b), *m*-SNGF/800 (c) and *m*-SNGF/1000 (d). The water contact angles of *m*-SNGF (e), *m*-SNGF/400 (f), *m*-SNGF/800 (g) and *m*-SNGF/1000 (h).

Table 1
The oil and water contact angles of the *o*-SNGF, *m*-SNGF and *p*-SNGF under different annealing temperature.

Annealing temperature	*m*-SNGF		*o*-SNGF or *p*-SNGF	
	water CA	oil CA	water CA	oil CA
RT	0°	0°	0°	0°
400 ℃	85°	0°	0°	0°
800 ℃	123°	0°	0°	0°
1000 ℃	147°	0°	0°	0°

CA: contact angle; RT: room temperature.

(pyrrolic-N, N-5, ~400.0 eV), in *m*-SNGF. After annealing at 400 °C or 800 °C, the N-A state decreases significantly, and the N atoms mainly exist in N-6 (~398.8 eV) and N-5 (~400.0 eV). Further increasing the annealing temperature, the N-A state further decreases, and N-Q (~400.9 eV) begins to appear. The N-Q is derived from the N atoms that replace the C atoms in the graphene hexagonal-ring, suggesting that the N atoms were incorporated into the C—C bonds of the graphene [35–37]. S 2p XPS spectra (Fig. S12 in Supporting information) show the S—O bonding state (oxidized sulfur, ~167.5 eV, ~168.8 eV) in *m*-SNGF. After annealing at 400 °C, two new peaks (S $2p_{3/2}$ at ~163.9 eV and S $2p_{1/2}$ at ~165.0 eV) appear, indicating the generation of S-T [38,39]. As the annealing temperature increases to 1000 °C, the SO_x component completely disappears, and the remaining S exists in S-T form. However, different from the N-doping, S atoms may not enter the graphene lattice because the bond length of C—S bond (d_{c-s} = 1.74 Å) is much larger than that of C—C bond (d_{c-c} = 1.42 Å) and C—N bond (d_{c-c} = 1.41 Å). Considering this, the S atoms existing in the S-T state are most probably immobilized at the edge or defect vacancy of graphene sheets [40,41].

The different chemical composition of the *m*-SNGF at different annealing temperatures renders the tunable wettability of this material. Table 1 well testifies this speculation. The water and oil CA indicate the *m*-SNGF is super-amphiphilic. After the annealing, the water CA gradually enhances from 0° to 147°, indicating that the wettability of the *m*-SNGF can be changed from amphiphilic to highly hydrophobic by controlling of annealing temperature. It is generally believed that 3D graphene-based materials are highly hydrophobic due to the large number of conjugated structures in graphene. However, for the SNGFs, -NH_2 and -SO_3H groups endow them with hydrophilicity. After annealing at high temperature, the N and S exist in N-5, N-6 N-Q, and S-T form, which attributes to the hydrophobicity. By comparison, the wettability of *o*-SNGF and *p*-SNGF cannot be changed from super-amphiphilic to hydrophobic by annealing treatment because the S and N still exist in hydrophilic S-O and N-A in *o*-SNGF or *p*-SNGF. Results demonstrate the wettability is greatly affected by the configuration of the dopant. Compared with configurational effects, the dosage of the dopant shows only slight effect on the wettability (Table S1 and Fig. S13 in Supporting information).

In summary, *m*-ABSA was selected as the dopant for the hydrothermal synthesis of N/S co-doped 3D graphene foams with tunable surface wettability. The effects of the configuration of ABSA on the morphology, chemical composition, and surface wettability of the resultant 3D SNGF have been systematically investigated. Results indicate that controllable wettability is achieved by adjusting the annealing temperature only when *m*-ABSA is used as the dopant because the bonded -SO_3H and -NH_2 groups further react with GO layer and dopes into the graphene lattice to form S-T state and N-6/ N-Q forms, respectively, in the annealing process. This work reveals the importance of dopant configurations in the resulting chemical composition and wettability of 3D graphene, which provides some constructive basis for dopant selection and manipulating the properties of 3D graphene foams.

Declaration of competing interest

The authors declare that they have no known competing financial interests or personal relationships that could have appeared to influence the work reported in this paper.

Acknowledgment

This research was financially supported by the National Natural Science Foundation of China (No. 21675133).

Appendix A. Supplementary data

Supplementary material related to this article can be found, in the online version, at doi:https://doi.org/10.1016/j.cclet.2020.02.053.

References

[1] L. Xia, B. Li, Y. Zhang, et al., Inorg. Chem. 58 (2019) 2257–2260.
[2] Y. Zhang, H. Du, Y. Ma, et al., Nano Res. 12 (2019) 919–924.
[3] H. Huang, F. Gong, Y. Wang, et al., Nano Res. 12 (2019) 1093–1098.
[4] H. Chen, X. Zhu, Hong Huang, et al., Chem. Commun. 55 (2019) 3152–3155.
[5] X. Wang, A.M. Jones, K.L. Seyler, et al., Nat. Nanotechnol. 10 (2015) 517–521.
[6] W. Wan, R. Zhang, Wei Li, et al., Environ. Sci: Nano 3 (2016) 107–113.
[7] Y. Xu, G. Shi, X. Duan, Acc. Chem. Res. 48 (2015) 1666–1675.
[8] J. Liang, Z. Zhao, Y. Tang, et al., Carbon 147 (2019) 206–213.
[9] K. Zhao, T. Zhang, H. Chang, et al., Sci. Adv. 5 (2019) eaav2589.
[10] Y. Men, J. Su, C. Huang, et al., Chin. Chem. Lett. 29 (2018) 1671–1674.
[11] X. Song, L. Lin, M. Rong, et al., Carbon 80 (2014) 174–182.
[12] M. Karthika, H. Chi, T. Li, H. Wang, S. Thomas, Compos. Part B: Eng. 173 (2019) 106978.
[13] D. Xu, J. Liu, P. Chen, et al., J. Mater. Chem. C 7 (2019) 3869–3880.
[14] C. Chen, X. Zhu, B. Chen, Environ. Sci. Technol. 53 (2019) 1509–1517.
[15] C. Liu, J. Yang, Y. Tang, et al., Colloids Surf. A: Physicochem. Eng. Aspects 468 (2015) 10–16.
[16] X. Wu, J. Wang, G. Zhang, et al., Appl. Catal. B: Environ. 201 (2017) 128–136.
[17] L. Li, B. Lia, J. Zhang, J. Mater. Chem. A 4 (2016) 512–518.
[18] S. Xia, J. Dong, Y. Chen, Y. Wang, X. Chen, Chin. Chem. Lett. 29 (2018) 107–110.
[19] Y. Zhang, J.Y. Zhu, H.B. Ren, Y.T. Bi, L. Zhang, Chin. Chem. Lett. 28 (2017) 935–942.
[20] H. Wang, T. Maiyalagan, X. Wang, ACS Catal. 2 (2012) 781–794.
[21] L. Ge, D. Wang, P. Yang, et al., Nanoscale 11 (2019) 17010–17017.
[22] Z.S. Wu, A. Winter, L. Chen, et al., Adv. Mater. 24 (2012) 5130–5135.
[23] X. Wang, G. Sun, P. Routh, et al., Chem. Soc. Rev. 43 (2014) 7067–7098.
[24] X. Yu, C. Pei, L. Feng, Chin. Chem. Lett. 30 (2019) 1121–1125.
[25] H.J. Ahn, I.H. Kim, J.C. Yoon, S.I. Kim, J.H. Jang, Chem. Commun. 50 (2014) 2412–2415.
[26] X. Song, Y. Chen, M. Rong, et al., Angew. Chem. 55 (2016) 3936–3941.
[27] Y. Chen, X. Song, T. Zhao, et al., J. Hazard. Mater. 343 (2018) 298–303.
[28] C.H. Choi, M.W. Chung, H.C. Kwon, S.H. Park, S.I. Woo, J. Mater. Chem. A 1 (2013) 3694–3699.
[29] W.S. Hummers, R.E. Offeman, J. Am. Chem. Soc. 80 (1958) 1339-1339.
[30] H.A. Becerril, J. Mao, Z. Liu, et al., ACS Nano 2 (2008) 463–470.
[31] A.C. Ferrari, J.C. Meyer, V. Scardaci, et al., Phys. Rev. Lett. 97 (2006) 187401.
[32] Z. Wang, H. Wang, Z. Zhang, X. Yang, G. Liu, Electrochim. Acta 120 (2014) 140–146.
[33] M. Zhang, H. Tao, Y. Liu, et al., ACS Sustain. Chem. Eng. 7 (2019) 3434–3442.
[34] Y. Shao, S. Zhang, M.H. Engelhard, et al., J. Mater. Chem. 20 (2010) 7491–7496.
[35] T.N. Edison, R. Atchudan, M.G. Sethuraman, J.J. Shim, Y.R. Lee, J. Photochem. Photobiol. B 161 (2016) 154–161.
[36] D. Zhang, L. Zheng, Y. Ma, et al., ACS Appl. Mater. Interfaces 6 (2014) 2657–2665.
[37] L. Duan, L. Zhao, H. Cong, et al., Small 15 (2019) 1804347.
[38] J. Chen, H. Zhang, P. Liu, et al., Carbon 92 (2015) 339–347.
[39] H. Huang, J. Zhu, W. Zhang, et al., Chem. Mater. 28 (2016) 1737–1745.
[40] S. Yang, L. Zhi, K. Tang, et al., Adv. Funct. Mater. 22 (2012) 3634–3640.
[41] J. Dai, J. Yuan, P. Giannozzi, Appl. Phys. Lett. 95 (2009) 232105.